ACS SENSORS

pubs.acs.org/acssensors

Article

Ratiometric pH Imaging Using a 1,2-Dioxetane Chemiluminescence Resonance Energy Transfer Sensor in Live Animals

Lucas S. Ryan, Jeni Gerberich, Uroob Haris, Daphne Nguyen, Ralph P. Mason, and Alexander R. Lippert*

Cite This: *ACS Sens.* 2020, 5, 2925–2932

Read Online

ACCESS | Metrics & More | Article Recommendations | Supporting Information

ABSTRACT: Regulation of physiological pH is integral for proper whole body and cellular function, and disruptions in pH homeostasis can be both a cause and effect of disease. In light of this, many methods have been developed to monitor pH in cells and animals. In this study, we report a chemiluminescence resonance energy transfer (CRET) probe **Ratio-pHCL-1**, composed of an acrylamide 1,2-dioxetane chemiluminescent scaffold with an appended pH-sensitive carbofluorescein fluorophore. The probe provides an accurate measurement of pH between 6.8 and 8.4, making it a viable tool for measuring pH in biological systems. Further, its ratiometric output is independent of confounding variables. Quantification of pH can be accomplished using both common luminescence spectroscopy and advanced optical imaging methods. Using an IVIS Spectrum, pH can be measured through tissue with **Ratio-pHCL-1**, which is shown *in vitro* and calibrated in sacrificed mouse models. Intraperitoneal injections of **Ratio-pHCL-1** into live mice show high photon outputs and consistent increases in the flux ratio when measured at pH 6, 7, and 8.

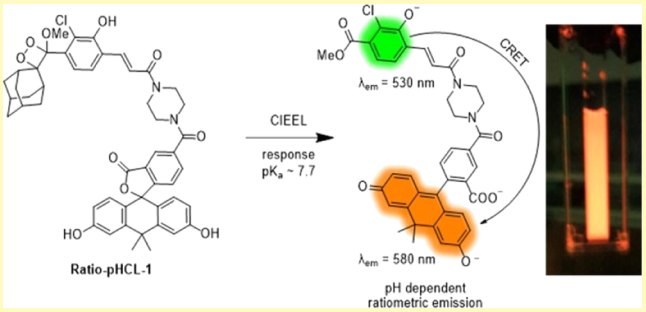

KEYWORDS: *chemiluminescence, 1,2 dioxetanes, CRET, in vivo imaging, pH imaging, ratiometric*

Regulation of physiological pH is an important factor for maintaining homeostasis. Whole body pH is regulated through numerous methods, including renal control of bicarbonate storage,[1] ammonia excretion,[2,3] CO_2 respiration,[4] and excretion of nonvolatile acids obtained from the diet.[3] These processes are controlled at a subcellular level through active transport by H^+-ATPase, passive transport by Na^+/HCO_3^- coporters,[5,6] and Cl^-/HCO_3^- and Na^+/H^+ antiporters.[7] Deviations in pH homeostasis can have major implications on cellular and whole body function and can be both a cause and effect of disease states. For example, untreated type 1 diabetes can result in ketoacidosis (a lowering of blood pH from overproduction of ketone bodies in β-oxidation of fatty acids) because of insulin deficiency.[8] Diseases associated with chronic inflammation display decreased pH levels and are positively correlated with increased cancer risk.[9] Extracellular pH is also altered in malignant tumors, as cancer cells generate excess lactate because of increased rates of glycolysis, even in the presence of sufficient O_2 needed for aerobic oxidation.[10] Because of their highly heterogenous microenvironments, tumors often display "hot spots" of increased acidity.[11] The ability to accurately quantify pH in a preclinical and clinical setting is critical to understand its impact on human health.

Current clinically relevant methods to measure pH include magnetic resonance imaging (MRI) techniques such as intra and extracellular ^{31}P MRI,[12] chemical exchange saturation transfer (CEST) MRI,[13−15] and other infused reporter molecules, notably ^{19}F-based agents, which can provide a large chemical shift range but often suffer from poor signal to noise.[16] These methods, however, can be time consuming and often require extensive training and expertise. Preclinical techniques for pH detection offer a more cost-effective approach to study pH in a laboratory setting. Insertion of pH microelectrodes has been used for preclinical measurement of pH in tumors[17,18] but is invasive and may disturb tumor physiology. Optical imaging using luminescent pH reporters has been extensively developed in recent years,[19−23] however, these compounds can be challenging to apply *in vivo* because of changes in luminescence intensity through tissue, hampering the ability to acquire accurate measurements. Ratiometric imaging agents circumvent this issue by providing an internal

Received: July 8, 2020
Accepted: August 24, 2020
Published: August 24, 2020

Scheme 1. Design and Mechanism of Ratio-pHCL-1

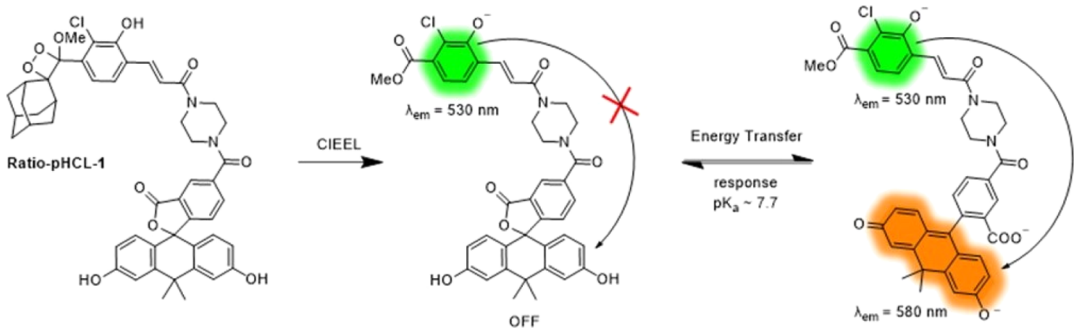

reference, and this technology has been utilized in GFP,[24] luciferase,[25] quantum dot,[26,27] and nanoparticle-based[28−30] agents for pH. However, no small-molecule 1,2-dioxetane ratiometric chemiluminescence agents for pH imaging have been made for *in vivo* application.

Chemiluminescence is light generation through an exothermic chemical reaction and is achieved through the breaking of chemical bonds. Specifically, 1,2-dioxetane compounds have garnered interest in this area because of their innate ability for triggered chemiluminescence emission via chemically initiated electron exchange luminescence (CIEEL).[31,32] This technology has been employed for imaging analytes by protecting the chemiluminophore with an analyte-selective trigger.[33] Upon deprotection of the dioxetane by the analyte, it will undergo CIEEL and luminesce. This strategy has been employed for detection of various analytes including hypoxia,[34−36] hydrogen sulfide,[37] peroxynitrite,[38] nitroxyl,[39] cathepsin B,[40] β-galactosidase,[41,42] formaldehyde,[43] and others.[44−52] Chemiluminescence provides many advantages compared to other optical methods *in vivo* by providing its own light source, thus attenuating autofluorescence and light scattering effects.[53] Chemiluminescent probes have also been shown to achieve much higher fold turn-on than comparable fluorophores.[39] Furthermore, they do not require expression of an enzyme for use, making them valuable standalone optical imaging tools as opposed to bioluminescence methods for monitoring pH.[25]

A major need for both chemiluminescence and fluorescence *in vivo* imaging is the development of luminophores with high quantum yields and red-shifted emission. Fluorophore development has flourished in this area, particularly with modifications to BODIPY,[54−57] xanthene,[58−63] and cyanine[64−66] cores. However, red-shifting emission of 1,2-dioxetane chemiluminescent compounds has been difficult. Arguably, the largest breakthrough in this area in recent years was the development of acryl-substituted phenoxy dioxetanes that greatly increased quantum yield and shifted emission to near 530 nm.[67] A dicyanomethylchromone-substituted scaffold has also been reported, providing the first 1,2-dioxetane to emit in the near-infrared (NIR) region[68] and has been successfully implemented in the detection of formaldehyde[43] and β-galactosidase.[42] One strategy to obtain bathochromic emission is by pairing donor and acceptor luminophores through resonance energy transfer mechanisms. Fluorescence resonance energy transfer (FRET) pairs have been rigorously vetted and are often used to detect macromolecular interactions in biochemical applications.[69] FRET also allows for fluorophores to be paired to dyes with sensing capabilities, thus providing ratiometric detection of analytes with the FRET pair.[70−73] It is currently known that 1,2-dioxetanes exhibit energy transfer capabilities,[50,74,75] but to our knowledge, no single-molecule 1,2-dioxetane ratiometric chemiluminescent probes for imaging pH have been developed. Here, we report the first single-molecule ratiometric chemiluminescence resonance energy transfer (CRET) sensor for pH imaging in living systems (Scheme 1).

EXPERIMENTAL SECTION

***In Vitro* Calibration of Ratio-pHCL-1.** Chemiluminescent emission spectra were acquired using a Hitachi F-7000 fluorescence spectrophotometer via the luminescence detection module and scanning luminescence emission from 400 to 900 nm in response to exposure of **Ratio-pHCL-1** to pH buffered solutions. A solution of 20 μM **Ratio-pHCL-1** in DMSO was added to a solution of 100 mM Tris, PBS, or carbonate buffers ranging from pH 6.81−8.42. For concentration dependence, 10, 20, and 40 μM **Ratio-pHCL-1** in 5% DMSO were subjected to 100 mM PBS buffered to pH 6.81, 7.45, and 8.02, respectively. For time dependence, 20 μM **Ratio-pHCL-1** in 5% DMSO was subjected to 100 mM PBS buffered to pH 6.81, 7.45, and 8.02, and the chemiluminescence emission spectra were measured at t = 0, 10, 20, and 30 min. For DMSO dependence, 20 μM **Ratio-pHCL-1** in a final concentration of 1, 5, or 10% DMSO was subjected to 100 mM PBS buffered to pH 6.81, 7.45, or 8.02. Each experiment was independently conducted three times at ambient temperature, and analysis of each experiment was conducted by dividing emission intensity values at 580 nm by emission intensity values at 530 nm from the emission plot.

Ratio-pHCL-1 Kinetics. Kinetics data were acquired using a Biotek Cytation 5 plate reader using the luminescence detection mode, end-point read type. The temperature was set at 37 °C under an ambient atmosphere. The gain was set at 135, and the read height was set at 4.5 mm. In a 96-well plate, 1.0 μL of 0.25 mM **Ratio-pHCL-1** was added to wells containing a solution of 237.5 μL 100 mM PBS (pH = 7.45) and 11.5 μL DMSO for a final concentration of 1.0 μM **Ratio-pHCL-1**, 5% DMSO. The plate was immediately placed into the plate reader and allowed to stir for 1 min. Luminescence readings were acquired every 2 min for 50 min.

Ratiometric pH Imaging. Chemiluminescence images were acquired with an IVIS Spectrum (Perkin Elmer, Waltham, MA) using the "Luminescent" and "Photograph" mode. For *in vitro* 96-well plate measurements, the exposure time was set as 0.5 s, binning was set to medium, F/stop was set as 4, FOV was set as C (12.9 cm), excitation was blocked, and the sequence was set for the emission mode, and images were acquired sequentially first using a 580 nm bandpass filter and then a 540 nm bandpass filter. A final concentration of 1 μM **Ratio-pHCL-1** was added to 100 mM buffer ranging from pH 6.81−8.42. All images were analyzed using Living Image software. Image analysis was carried out by setting individual ROIs to each well for both 580 and 540 nm filter images. ROIs were then measured, which gave a total flux (p/s) for each ROI, and the flux value at 580 nm was divided by the flux at 540 nm for each well. For sacrificed mouse imaging, 950 μL of 1.0 M PBS (pH 5.99−7.99) was injected into the peritoneal cavity of recently sacrificed CL6B57

https://dx.doi.org/10.1021/acssensors.0c01393
ACS Sens. 2020, 5, 2925−2932

Scheme 2. Synthesis of Ratio-pHCL-1

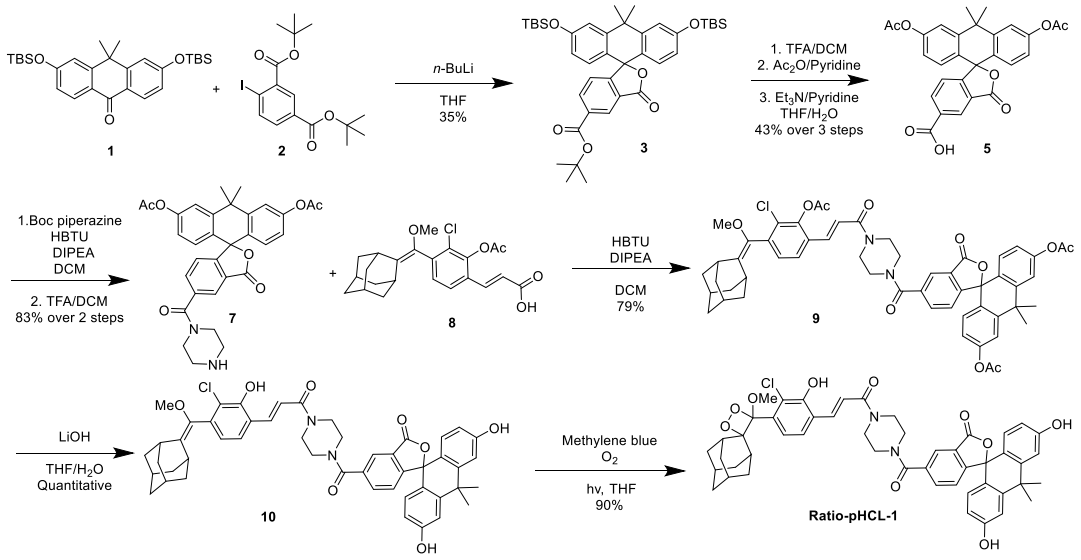

mice aged 6−12 weeks old, and then, 50 μL of 400 μM **Ratio-pHCL-1** in DMSO was injected shortly after to achieve an approximate final concentration of 20 μM **Ratio-pHCL-1** with 5% DMSO. For live mouse imaging, 475 μL of freshly prepared 20 μM **Ratio-pHCL-1** dissolved in 1.0 M PBS (pH 5.99−7.99, 5% DMSO) was directly injected into the peritoneal cavity of male BALB-C mice aged to 4.5 months. The mice were imaged immediately after injection of the solution with 580 and 540 nm filters with capture setting set to autoexposure and FOV set to C (12.9 cm).

RESULTS

In previous work, we demonstrated ratiometric quantification of pH *in vitro* using the light emission from 1,2-dioxetane chemiluminophores.[75] These studies, however, required the addition of the pH-sensitive dye seminaptharhodafluor (SNARF) coupled with the addition of a chemiluminescence enhancer solution and were not viable for *in vivo* application. We sought a molecule with increased chemiluminescence quantum yields, red-shifted emission, and a pH-sensitive fluorophore directly conjugated to the dioxetane scaffold for increased energy transfer efficiency and ease of use. Inspired by previously reported pH-sensitive carbofluoresceins with fluorescence emissions near 580 nm that interconvert between an open, fluorescent form at high pH and a colorless, nonfluorescent closed form under acidic conditions,[58] we postulated that conjugation of this fluorophore to the dioxetane scaffold could provide a ratiometric measure of pH (Scheme 1).

Synthesis of **Ratio-pHCL-1** began with the synthesis of *tert*-butyl-dimethylsilyl ether (TBS)-protected anthrone **1** from reported literature procedures (Scheme 2).[58] Because of difficulties in conjugation of the top segment of the fluorophore to **1** using reported Grignard metathesis to form the carbofluorescein unit, we decided to explore alternative methods. It has been shown that iodo compounds react faster than their bromo counterparts during lithium halogen exchange,[76] so we proceeded to synthesize 2-iodo-*tert*-butyl-isophthalate **2** from commercially available 2-aminoisophthalic acid.[77] TBS-protected carbofluorescein **3** was successfully formed in 35% yield by premixing **1** and **2**, purging the mixture three times under vacuum, addition of dry THF, and then addition of 1 equivalent of *n*-BuLi at 0 °C. This protocol proved to be general and could be used for preparing other xanthene scaffolds, including silicon rhodamines (Scheme S1). We postulate that the faster rate of lithium−iodine exchange compared to nucleophilic addition of *n*-BuLi to the anthrone enables the use of *n*-BuLi as a safer alternative to *tert*-BuLi.

Compound **3** was further modified in order to conjugate it to the chemiluminescent scaffold. We simultaneously deprotected both the TBS and *tert*-butyl ester-protecting groups with trifluoroacetic acid (TFA). The xanthene phenols were protected with acetic anhydride to obtain **5**, but it was noticed that a less polar spot as shown by thin layer chromatography (TLC) also formed during the reaction, which was presumed to be the mixed anhydride product. This spot disappeared by subjecting the crude mixture to 1 equiv of triethylamine and five equivalents of pyridine in a 1:1 THF/H_2O mixture to produce **5** in a 64% yield. We then appended *tert*-butyl piperazine-1-carboxylate to **5** and subsequently deprotected the *tert*-butyloxy carbamate with TFA to obtain amine **7**.

The final steps were to conjugate the chemiluminescent scaffold and carbofluorescein together, deprotect to form the free phenol precursor, and form the dioxetane compound. We decided to also use an acetate protection strategy to form compound **8** from literature-reported compound **S7** in 64% yield (Scheme S1). This was advantageous to preparation of the final probe because all three acetates could be deprotected in a single step. We proceeded to conjugate **7** and **8** together via 2-(1*H*-benzotriazol-1-yl)-1,1,3,3-tetramethyluronium hexafluorophosphate (HBTU) coupling to form triacetate **9**, which was subsequently deprotected with 1 M LiOH to form precursor **10** in quantitative yield. **10** underwent a light-mediated [2 + 2] cycloaddition with singlet oxygen generated with methylene blue as a photosensitizer to obtain **Ratio-pHCL-1** in 90% yield.

Upon synthesis of **Ratio-pHCL-1**, we proceeded to characterize its properties *in vitro*. We verified the absorbance spectrum of 100 μM **Ratio-pHCL-1** (100 mM PBS, pH 7.45, 5% DMSO) against the chemiluminescence emission spectrum of the reported methyl acrylate dioxetane (20 μM, 100 mM PBS, pH 7.45, 5% DMSO) (Figure S1).[67] The emission wavelength of the methyl acrylate dioxetane centered at 530 nm coincides with an absorbance maximum of **Ratio-pHCL-1**

https://dx.doi.org/10.1021/acssensors.0c01393
ACS Sens. 2020, 5, 2925−2932

at 544 nm, indicating strong spectral overlap between the chemiluminescence emission profile of the dioxetane donor and absorption of the carbofluorescein acceptor. We measured the chemiluminescence emission of 20 μM **Ratio-pHCL-1** (100 mM PBS or Tris, pH 6.81−8.42, 5% DMSO). Analysis of the emission spectra over this pH range revealed one peak centered at 580 nm attributed to luminescence from the carbofluorescein scaffold and a shoulder around 530 nm corresponding to CIEEL from the chemiluminescent scaffold (Figure 1A). As the pH of the system is increased, emission at

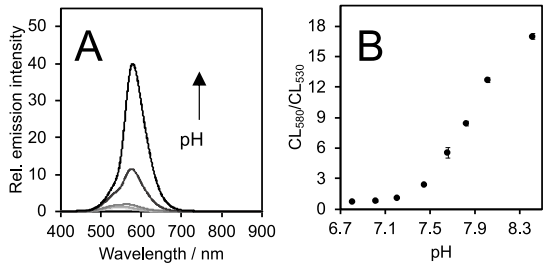

Figure 1. pH-dependent (A) chemiluminescence emission spectra of 20 μM **Ratio-pHCL-1** and 5% DMSO in 100 mM PBS buffer from pH 6.81−7.63 and (B) ratio of chemiluminescence emission intensities at 580 nm and 530 nm of 20 μM **Ratio-pHCL-1** and 5% DMSO in aqueous buffer (pH = 6.81−8.44). All measurements were taken in 100 mM PBS or 100 mM Tris, and measurements were taken 20 s after mixing. Error bars are ±SD from n = 3 independent experiments.

both peaks increases because of increased concentration of phenolate over phenol; however, luminescence intensity from the carbofluorescein increases in this system to a greater extent than the luminescence from the chemiluminophore; analysis shows a 24-fold change in the ratio of emission intensities at 580 nm over 530 nm from pH 6.81−8.42 (Figure 1B), demonstrating that the emission spectrum of **Ratio-pHCL-1** is pH dependent. We then measured decomposition kinetics of 1.0 μM **Ratio-pHCL-1** (100 mM PBS, pH 7.45, 5% DMSO, 37 °C). Figure S3 shows an observed peak emission at the initial time point, followed by a steady decline to baseline values over 50 min.

We subjected **Ratio-pHCL-1** to variables to confirm that its ratiometric response is independent of testing conditions. We first examined changes in emission spectra upon changing the concentration of **Ratio-pHCL-1** (Figure 2). We tested 10, 20,

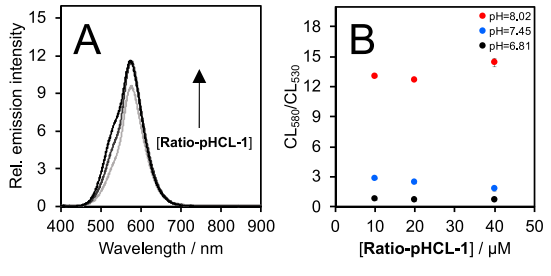

Figure 2. Dependence of chemiluminescence emission on the concentration of **Ratio-pHCL-1**. (A) Emission spectra at pH 7.45 and (B) ratio of the chemiluminescence emission intensity at 580 and 530 nm of 10, 20, and 40 μM **Ratio-pHCL-1** in PBS buffer at pH 6.81 (light gray trace), 7.45 (dark gray trace), and 8.02 (black trace) containing 5% DMSO. All measurements were taken 20 s after mixing. Error bars are ±SD from n = 3 independent experiments.

and 40 μM **Ratio-pHCL-1** (100 mM PBS, pH 6.81−8.02, 5% DMSO). **Ratio-pHCL-1** shows a dose-dependent increase in emission intensity as concentration increases, however, both peaks increase proportionally (Figure 2A). Analysis of the ratio of emission intensities at 580 and 530 nm plotted versus the concentration of **Ratio-pHCL-1** reveals that the signal remains relatively consistent despite changes in its concentration (Figure 2B), only showing a slight downward trend with increasing concentration at pH 7.45. We then subjected 20 μM **Ratio-pHCL-1** to varying DMSO concentrations (100 mM PBS, pH 6.81−8.02, 1−10% DMSO). **Ratio-pHCL-1** showed a dose-dependent increase in overall emission intensity with increasing DMSO concentration, likely because of increases in chemiluminescence quantum yield (Figure 3A). However,

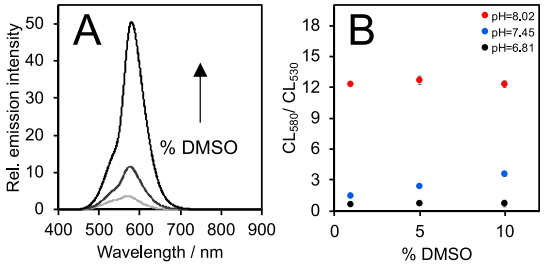

Figure 3. Dependence of chemiluminescence emission on the concentration of DMSO. (A) Emission spectra at pH 7.45 with 1, 5, or 10% DMSO and (B) ratio of the chemiluminescence emission intensity at 580 and 530 nm of 20 μM **Ratio-pHCL-1** in PBS buffer at pH 6.81 (light gray trace), 7.45 (dark gray trace), and 8.02 (black trace) containing 1, 5 or 10% DMSO. All measurements were taken 20 s after mixing. Error bars are ±SD from n = 3 independent experiments.

changes in DMSO concentration did not greatly change the ratio of emission intensities at 580 and 530 nm, albeit showing a slight upward trend in chemiluminescence emission at pH 7.45 (Figure 3B).

We then measured 20 μM **Ratio-pHCL-1** (100 mM PBS, pH 6.81−8.02) from 0 to 30 min with 10 min intervals to test probe stability over time. Figure 4A reveals that the overall chemiluminescence intensity decreases over time, as was expected from free phenol dioxetane kinetics. Plotting the ratio of emission intensities at 580 nm over 530 nm does reveal small changes in emission intensities over time, with a slight upward trend at pH 7.45 and a more pronounced downward trend at pH 8.02 over a 30 min period (Figure 4B), likely

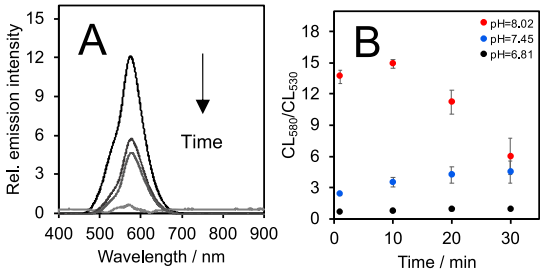

Figure 4. Time-dependent (A) emission spectrum at pH 7.45 and (B) ratio of the chemiluminescence emission intensities at 580 and 530 nm of 20 μM **Ratio-pHCL-1** in 100 mM PBS at pH 6.81 (light gray trace), 7.45 (dark gray trace), and 8.02 (black trace) containing 5% DMSO. All measurements were taken 20 s after mixing. Error bars are ±SD from n = 3 independent experiments.

https://dx.doi.org/10.1021/acssensors.0c01393
ACS Sens. 2020, 5, 2925−2932

because of more rapid decomposition kinetics at this pH. These variations indicate that care should be taken when using **Ratio-pHCL-1** at higher pH values. Imaging experiments should be performed quickly after injection or at well-defined time-points to ensure equal comparisons, especially when performing experiments at elevated pH.

Next, we examined the behavior of **Ratio-pHCL-1** in biological systems. Cellular uptake of 20 μM **Ratio-pHCL-1** in A549 cells was examined over an 80 min period (Figure S4), and changes in fluorescence were monitored using a fluorescence microscope. After washing the cells, increased intracellular fluorescence could be seen from the acrylamide and carbofluorescein motifs by using GFP and RFP filter sets, respectively. These results show that **Ratio-pHCL-1** can cross the cellular membrane and accumulate inside cells. We proceeded to measure cell viability of **Ratio-pHCL-1** (Figure S5) using a 3-(4,5-dimethylthiazol-2-yl)-2,5-diphenyltetrazolium bromide assay. Cells maintained at least 67% viability when exposed to 1−250 μM **Ratio-pHCL-1**.

Upon completion of the *in vitro* spectrophotometry experiments and cellular studies, we confirmed the feasibility of quantitative pH imaging using **Ratio-pHCL-1** in an IVIS Spectrum. We subjected **Ratio-pHCL-1** to buffered solutions (100 mM PBS, pH 6.81−8.42, 5% DMSO) and took sequential images using the available 580 and 540 nm bandpass filters and 0.5 s exposure time. Four independent experiments were completed, and each buffered solution was measured with three technical replicates per experiment. A solution of 20 μM **Ratio-pHCL-1** was too bright and saturated the images at this setting, so the concentration was lowered to 1.0 μM. Images of the plate taken with average radiance heat maps set to 10^9 photons sec^{-1} cm^{-2} sr^{-1} for the 580 nm filter and 10^8 photons sec^{-1} cm^{-2} sr^{-1} for the 540 nm filter (Figure 5A,B, respectively) show that average radiance increases with

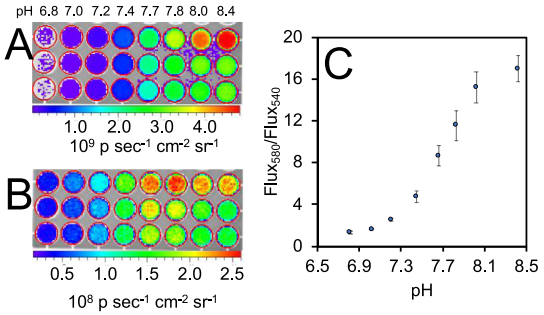

Figure 5. Chemiluminescence intensity images of the pH-dependent emission of 1 μM **Ratio-pHCL-1** in 100 mM PBS or Tris buffer (pH 6.81−8.42) containing 5% DMSO using(A) 580 nm bandpass filter or (B) 540 nm bandpass filter in an IVIS Spectrum. (C) Ratio of total flux (p/s) at 580 and 540 nm. n = 12 technical replicates across four independent experiments, and error bars are ±SD.

pH on both filter settings. Plotting the flux (photons/s) at 580 nm over flux at 540 nm for each well shows an increase in the ratio between the two wavelengths as the pH increases, and the generated curve agrees well with our previous *in vitro* calibration. The imaging data, as shown in Figure 5, were used to determine the observed pK_a of the response. It was found that a modified Henderson−Hasselbalch equation with the inclusion of a Hill coefficient[78] was needed to fit the data. The observed pK_a of the response was determined to be 7.70 ± 0.03 with a Hill coefficient of 2.21 ± 0.32 (S.D., n = 12), indicating cooperativity between multiple protonation sites. We then confirmed that a ratiometric chemiluminescence response could be measured through a tissue surrogate by placing a 2.8 mm thick slice of bologna (Kroger, Dallas, TX) atop a 96-well plate loaded with 20 μM **Ratio-pHCL-1** in buffered solutions (100 mM PBS or Tris, pH 6.81−8.42, 5% DMSO) and took sequential 580 and 540 nm filtered images with 10.0 s exposure times (Figure S6), which clearly showed penetration through this tissue surrogate.

Finally, we investigated the response of **Ratio-pHCL-1** in animal models. First, we did a proof-of-principle experiment in recently sacrificed C57BL6 mice, which were given 950 μL intraperitoneal (IP) injections of 1.0 M PBS (pH 5.99−7.99) and then subsequently given 50 μL of IP injections of 400 μM **Ratio-pHCL-1** to achieve a theoretical final concentration of 20 μM **Ratio-pHCL-1** with 5% DMSO in the injection volume and imaged with 580 and 540 nm filters. With radiance heat maps of both 580 and 540 nm images set to 10^9 p sec^{-1} cm^{-2} sr^{-1} (Figure S7A,B), there is a clear increase in flux from the 580 nm image from pH 6.0−8.0, with a less pronounced increase in the 540 nm image over the same pH range. Plotting total flux at 580 nm over flux at 540 nm shows an increase in the ratio of total flux from both filter sets with increasing pH (Figure S7C), demonstrating that **Ratio-pHCL-1** can discern changes in pH in the peritoneal cavity of mice. Confident with these results, we moved to *in vivo* measurement of pH in the peritoneal cavity of mice. Live male BALB-C mice aged 4.5 months were given 475 μL of injections of 20 μM **Ratio-pHCL-1** (1.0 M PBS, pH 5.99−7.99, 5% DMSO) and immediately imaged with 580 and 540 nm filters. With radiance heat maps set to 10^8 p sec^{-1} cm^{-2} sr^{-1} for both images, there are pronounced increases in overall intensity through both filter sets across the pH gradient and discernible changes in flux output in each mouse from the 580 nm filter over the 540 nm filter images (Figure 6A,B). Indeed, the flux ratio between these filter sets increases with increasing pH (Figure 6C). This result was consistent across three independent experiments (Figure S8), demonstrating the robustness of using **Ratio-pHCL-1** for *in vivo* chemiluminescence pH imaging.

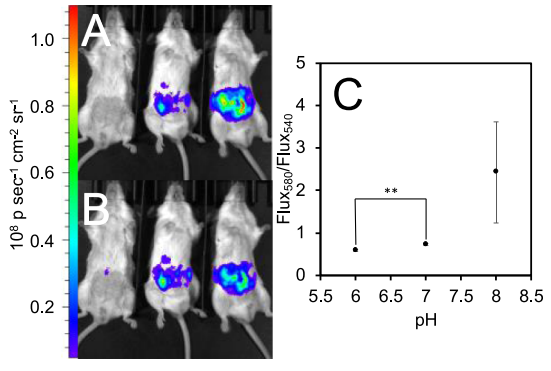

Figure 6. Chemiluminescence images of the pH-dependent emission of 475 μL of 20 μM **Ratio-pHCL-1** (1.0 M PBS, pH 5.99−7.99, 5% DMSO) injected into the peritoneal cavity of male BALB-C mice aged to 4.5 months using a (A) 580 nm bandpass filter or (B) 540 nm bandpass filter in an IVIS Spectrum. (C) Ratio of total flux (p/s) at 580 and 540 nm. n = 3 biological replicates for each pH tested, and error bars are ±SD. Statistical significance was assessed using two-tailed Student's t-test. **p < 0.005 (n = 3 biological replicates).

https://dx.doi.org/10.1021/acssensors.0c01393
ACS Sens. 2020, 5, 2925−2932

CONCLUSIONS

In summary, we have developed the first single-molecule 1,2-dioxetane ratiometric chemiluminescence probe for imaging pH in live animals. This was synthetically achieved by attaching a pH-sensitive carbofluorescein to the chemiluminescent acrylamide dioxetane scaffold via a piperazine linker. **Ratio-pHCL-1** generates light through CIEEL decomposition and concomitant pH-dependent emission from the appended fluorophore through a CRET mechanism. **Ratio-pHCL-1** is highly accurate *in vitro*, providing quantitative measurement of pH in biological ranges. Its ratiometric output is stable to confounding variables and provides a similar response when collected through optical imaging methods. We note that the observed pK_a of the response is 7.7, which is slightly higher than the ideal range of 6.8−7.4 for biological imaging. Nonetheless, a pH-dependent ratiometric emission is also reported in the peritoneal cavity of sacrificed mice, and robust *in vivo* measurement of pH in live mouse models has been accomplished. We report flux outputs of more than 10^8 to 10^9 p/s from 20 μM **Ratio-pHCL-1** through biological tissue, which exceeds the photon flux of most reported chemiluminescence agents. This increase in brightness is achieved through use of an unmasked phenoxy dioxetane that provides instantaneous decomposition and light output. This shows a clear advantage to chemiluminescence detection using unmasked dioxetanes—they have the potential for much higher signal intensity in biological settings. This methodology can be applied to highly sensitive quantitation of other analytes and provides a foundation for *in vivo* ratiometric imaging with 1,2-dioxetanes.

ASSOCIATED CONTENT

Supporting Information

The Supporting Information is available free of charge at https://pubs.acs.org/doi/10.1021/acssensors.0c01393.

Synthetic and experimental details, supplementary figures, and scanned spectral data (PDF)

AUTHOR INFORMATION

Corresponding Author

Alexander R. Lippert − *Department of Chemistry, Center for Drug Discovery, Design, and Delivery (CD4), and Center for Global Health Impact (CGHI), Southern Methodist University, Dallas, Texas 75275-0314, United States;* orcid.org/0000-0003-4396-0848; Email: alippert@smu.edu; Fax: 214-768-4089

Authors

Lucas S. Ryan − *Department of Chemistry, Southern Methodist University, Dallas, Texas 75275-0314, United States*

Jeni Gerberich − *Prognostic Imaging Research Laboratory (PIRL), Pre-clinical Imaging Section, Department of Radiology, UT Southwestern Medical Center, Dallas, Texas 75390-9058, United States*

Uroob Haris − *Department of Chemistry, Southern Methodist University, Dallas, Texas 75275-0314, United States*

Daphne Nguyen − *Department of Chemistry, Southern Methodist University, Dallas, Texas 75275-0314, United States*

Ralph P. Mason − *Prognostic Imaging Research Laboratory (PIRL), Pre-clinical Imaging Section, Department of Radiology, UT Southwestern Medical Center, Dallas, Texas 75390-9058, United States*

Complete contact information is available at: https://pubs.acs.org/10.1021/acssensors.0c01393

Author Contributions

The manuscript was written through contributions of all the authors. All the authors have given approval to the final version of the manuscript.

Notes

The authors declare the following competing financial interest(s): A.R.L. discloses a financial stake in BioLum Sciences, LLC, a company developing point-of-care medical devices.

ACKNOWLEDGMENTS

This work was supported by the National Science Foundation under CHE 1653474, and optical imaging was performed using an IVIS purchased under NIH 1S10RR024757 and supported by NIH P30 CA142543. We acknowledge Eric Weaver (UT Arlington) for assistance with mass spectrometry.

REFERENCES

(1) Hamm, L. L.; Nakhoul, N.; Hering-Smith, K. S. Acid-Base Homeostasis. *Clin. J. Am. Soc. Nephrol.* **2015**, *10*, 2232−2242.

(2) Weiner, I. D.; Hamm, L. L. Molecular Mechanisms of Renal Ammonia Transport. *Annu. Rev. Physiol.* **2007**, *69*, 317−340.

(3) Koeppen, B. M. The Kidney and Acid-Base Regulation. *Adv. Physiol. Educ.* **2009**, *33*, 275−281.

(4) Ruffin, V. A.; Salameh, A. I.; Boron, W. F.; Parker, M. D. Intracellular PH Regulation by Acid-Base Transporters in Mammalian Neurons. *Front. Physiol.* **2014**, *5*, 1−11.

(5) Boron, W. F. Regulation of Intracellular PH. *Adv. Physiol. Educ.* **2004**, *28*, 160−179.

(6) Aalkjaer, C.; Boedtkjer, E.; Choi, I.; Lee, S. Cation-Coupled Bicarbonate Transporters. *Compr. Physiol.* **2014**, *4*, 1605−1637.

(7) Aoi, W.; Marunaka, Y. Importance of PH Homeostasis in Metabolic Health and Diseases: Crucial Role of Membrane Proton Transport. *BioMed Res. Int.* **2014**, *2014*, 598986.

(8) Trachtenbarg, D. E. Diabetic Ketoacidosis. *Am. Fam. Physician* **2005**, *71*, 1705−1714.

(9) Boedtkjer, E.; Pedersen, S. F. The Acidic Tumor Microenvironment as a Driver of Cancer. *Annu. Rev. Physiol.* **2020**, *82*, 103−126.

(10) Heiden, M. G. V.; Cantley, L. C.; Thompson, C. B. Understanding the Warburg Effect: The Metabolic Requirements of Cell Proliferation. *Science* **2009**, *329*, 029−1033.

(11) Rohani, N.; Hao, L.; Alexis, M. S.; Joughin, B. A.; Krismer, K.; Moufarrej, M. N.; Soltis, A. R.; Lauffenburger, D. A.; Yaffe, M. B.; Burge, C. B.; et al. Acidification of Tumor at Stromal Boundaries Drives Transcriptome Alterations Associated with Aggressive Phenotypes. *Cancer Res.* **2019**, *79*, 1952−1966.

(12) Robey, I. F.; Baggett, B. K.; Kirkpatrick, N. D.; Roe, D. J.; Dosescu, J.; Sloane, B. F.; Hashim, A. I.; Morse, D. L.; Raghunand, N.; Gatenby, R. A.; et al. Bicarbonate Increases Tumor PH and Inhibits Spontaneous Metastases. *Cancer Res.* **2009**, *69*, 2260−2268.

(13) Jin, T.; Wang, P.; Hitchens, T. K.; Kim, S.-G.; Kim, S. G. Enhancing Sensitivity of PH-Weighted MRI with Combination of Amide and Guanidyl CEST. *Neuroimage* **2017**, *157*, 341−350.

(14) Wu, Y.; Zhou, I. Y.; Igarashi, T.; Longo, D. L.; Aime, S.; Sun, P. Z. A Generalized Ratiometric Chemical Exchange Saturation Transfer (CEST) MRI Approach for Mapping Renal PH Using Iopamidol. *Magn. Reson. Med.* **2018**, *79*, 1553−1558.

(15) Pavuluri, K.; McMahon, M. T. PH Imaging Using Chemical Exchange Saturation Transfer (CEST) MRI. *Isr. J. Chem.* **2017**, *57*, 862−887.

(16) Mason, R. P. Transmembrane PH Gradients In Vivo: Measurements Using Fluorinated Vitamin B6 Derivatives. *Curr. Med. Chem.* **1999**, *6*, 491−499.

(17) Jähde, E.; Rajewsky, M. F. Sensitization of Clonogenic Malignant Cells to Hyperthermia by Glucose-Mediated, Tumor-Selective PH Reduction. *J. Cancer Res. Clin. Oncol.* **1982**, *104*, 23−30.
(18) Engin, K.; Leeper, D. B.; Thistlethwaite, A. J.; Tupchong, L.; Phil, D.; McFarlane, J. D. Tumor Extracellular PH as a Prognostic Factor in Thermoradiotherapy. *Int. J. Radiat. Oncol., Biol., Phys.* **1994**, *29*, 125−132.
(19) Aggarwal, K.; Khurana, J. M. Indeno-Furan Based Colorimetric and on-off Fluorescent PH Sensors. *J. Photochem. Photobiol., A* **2015**, *307-308*, 23−29.
(20) Li, Z.; Li, L.-J.; Sun, T.; Liu, L.; Xie, Z. Benzimidazole-BODIPY as Optical and Fluorometric PH Sensor. *Dyes Pigm.* **2016**, *128*, 165−169.
(21) Qi, J.; Liu, D.; Liu, X.; Guan, S.; Shi, F.; Chang, H.; He, H.; Yang, G. Fluorescent PH Sensors for Broad-Range PH Measurement Based on a Single Fluorophore. *Anal. Chem.* **2015**, *87*, 5897−5904.
(22) Xu, X.-Y.; Yan, B. An Efficient and Sensitive Fluorescent PH Sensor Based on Amino Functional Metal-Organic Frameworks in Aqueous Environment. *Dalton Trans.* **2016**, *45*, 7078−7084.
(23) Richardson, D. S.; Gregor, C.; Winter, F. R.; Urban, N. T.; Sahl, S. J.; Willig, K. I.; Hell, S. W. SRpHi Ratiometric PH Biosensors for Super-Resolution Microscopy. *Nat. Commun.* **2017**, *8*, 577.
(24) Hanson, G. T.; McAnaney, T. B.; Park, E. S.; Rendell, M. E. P.; Yarbrough, D. K.; Chu, S.; Xi, L.; Boxer, S. G.; Montrose, M. H.; Remington, S. J. Green Fluorescent Protein Variants as Ratiometric Dual Emission pH Sensors. 1. Structural Characterization and Preliminary Application†. *Biochemistry* **2002**, *41*, 15477−15488.
(25) Zhang, Y.; Xie, Q.; Robertson, J. B.; Johnson, C. H. pHlash: A New Genetically Encoded and Ratiometric Luminescence Sensor of Intracellular pH. *PLoS One* **2012**, *7*, No. e43072.
(26) Pratiwi, F. W.; Hsia, C.-H.; Kuo, C. W.; Yang, S.-M.; Hwu, Y.-K.; Chen, P. Construction of Single Fluorophore Ratiometric PH Sensors Using Dual-Emission Mn2+-Doped Quantum Dots. *Biosens. Bioelectron.* **2016**, *84*, 133−140.
(27) Jin, T.; Sasaki, A.; Kinjo, M.; Miyazaki, J. A Quantum Dot-Based Ratiometric PH Sensor. *Chem. Commun.* **2010**, *46*, 2408−2410.
(28) Shi, W.; Li, X.; Ma, H. A Tunable Ratiometric Ph Sensor Based on Carbon Nanodots for the Quantitative Measurement of the Intracellular PH of Whole Cells. *Angew. Chem., Int. Ed.* **2012**, *51*, 6432−6435.
(29) Ma, T.; Hou, Y.; Zeng, J.; Liu, C.; Zhang, P.; Jing, L.; Shangguan, D.; Gao, M. Dual-Ratiometric Target-Triggered Fluorescent Probe for Simultaneous Quantitative Visualization of Tumor Microenvironment Protease Activity and PH in Vivo. *J. Am. Chem. Soc.* **2018**, *140*, 211−218.
(30) Lei, J.; Wang, L.; Zhang, J. Ratiometric PH Sensor Based on Mesoporous Silica Nanoparticles and Förster Resonance Energy Transfer. *Chem. Commun.* **2010**, *46*, 8445−8447.
(31) Augusto, F. A.; De Souza, G. A.; de Souza Júnior, S. P.; Khalid, M.; Baader, W. J. Efficiency of Electron Transfer Initiated Chemiluminescence. *Photochem. Photobiol.* **2013**, *89*, 1299−1317.
(32) Vacher, M.; Fdez. Galván, I.; Ding, B.-W.; Schramm, S.; Berraud-Pache, R.; Naumov, P.; Ferré, N.; Liu, Y.-J.; Navizet, I.; Roca-Sanjuán, D.; et al. Chemi- and Bioluminescence of Cyclic Peroxides. *Chem. Rev.* **2018**, *118*, 6927−6974.
(33) Bezner, B. J.; Ryan, L. S.; Lippert, A. R. Reaction-Based Luminescent Probes for Reactive Sulfur, Oxygen, and Nitrogen Species: Analytical Techniques and Recent Progress. *Anal. Chem.* **2020**, *92*, 309−326.
(34) Ryan, L. S.; Gerberich, J.; Cao, J.; An, W.; Jenkins, B. A.; Mason, R. P.; Lippert, A. R. Kinetics-Based Measurement of Hypoxia in Living Cells and Animals Using an Acetoxymethyl Ester Chemiluminescent Probe. *ACS Sens.* **2019**, *4*, 1391−1398.
(35) Cao, J.; Campbell, J.; Liu, L.; Mason, R. P.; Lippert, A. R. In Vivo Chemiluminescent Imaging Agents for Nitroreductase and Tissue Oxygenation. *Anal. Chem.* **2016**, *88*, 4995−5002.
(36) Sun, J.; Hu, Z.; Wang, R.; Zhang, S.; Zhang, X. A Highly Sensitive Chemiluminescent Probe for Detecting Nitroreductase and Imaging in Living Animals. *Anal. Chem.* **2019**, *91*, 1384−1390.
(37) Cao, J.; Lopez, R.; Thacker, J. M.; Moon, J. Y.; Jiang, C.; Morris, S. N. S.; Bauer, J. H.; Tao, P.; Mason, R. P.; Lippert, A. R. Chemiluminescent Probes for Imaging H2S in Living Animals. *Chem. Sci.* **2015**, *6*, 1979−1985.
(38) Cao, J.; An, W.; Reeves, A. G.; Lippert, A. R. A Chemiluminescent Probe for Cellular Peroxynitrite Using a Self-Immolative Oxidative Decarbonylation Reaction. *Chem. Sci.* **2018**, *9*, 2552−2558.
(39) An, W.; Ryan, L. S.; Reeves, A. G.; Bruemmer, K. J.; Mouhaffel, L.; Gerberich, J. L.; Winters, A.; Mason, R. P.; Lippert, A. R. A Chemiluminescent Probe for HNO Quantification and Real-Time Monitoring in Living Cells. *Angew. Chem., Int. Ed.* **2019**, *58*, 1361−1365.
(40) Roth-Konforti, M. E.; Bauer, C. R.; Shabat, D. Unprecedented Sensitivity in a Probe for Monitoring Cathepsin B: Chemiluminescence Microscopy Cell-Imaging of a Natively Expressed Enzyme. *Angew. Chem., Int. Ed.* **2017**, *56*, 15633−15638.
(41) Liu, L.; Mason, R. P. Imaging β-Galactosidase Activity in Human Tumor Xenografts and Transgenic Mice Using a Chemiluminescent Substrate. *PLoS One* **2010**, *5*, No. e12024.
(42) Zhang, Y.; Yan, C.; Wang, C.; Guo, Z.; Liu, X.; Zhu, W. H. A Sequential Dual-Lock Strategy for Photoactivatable Chemiluminescent Probes Enabling Bright Duplex Optical Imaging. *Angew. Chem., Int. Ed.* **2020**, *59*, 9059−10.
(43) Bruemmer, K. J.; Green, O.; Su, T. A.; Shabat, D.; Chang, C. J. Chemiluminescent Probes for Activity-Based Sensing of Formaldehyde Released from Folate Degradation in Living Mice. *Angew. Chem., Int. Ed.* **2018**, *57*, 7508−7512.
(44) Huang, J.; Lyu, Y.; Li, J.; Cheng, P.; Jiang, Y.; Pu, K. A Renal-Clearable Duplex Optical Reporter for Real-Time Imaging of Contrast-Induced Acute Kidney Injury. *Angew. Chem., Int. Ed.* **2019**, *58*, 17796−17804.
(45) Gnaim, S.; Scomparin, A.; Das, S.; Blau, R.; Satchi-Fainaro, R.; Shabat, D. Direct Real-Time Monitoring of Prodrug Activation by Chemiluminescence. *Angew. Chem., Int. Ed.* **2018**, *57*, 9033−9037.
(46) Roth-Konforti, M.; Green, O.; Hupfeld, M.; Fieseler, L.; Heinrich, N.; Ihssen, J.; Vorberg, R.; Wick, L.; Spitz, U.; Shabat, D. Ultrasensitive Detection of Salmonella and Listeria Monocytogenes by Small-Molecule Chemiluminescence Probes. *Angew. Chem.* **2019**, *131*, 10469−10475.
(47) Das, S.; Ihssen, J.; Wick, L.; Spitz, U.; Shabat, D. Chemiluminescence Carbapenem-based Molecular Probe for Detection of Carbapenemase Activity in Live Bacteria. *Chem.—Eur. J.* **2020**, *26*, 3647−3652.
(48) Son, S.; Won, M.; Green, O.; Hananya, N.; Sharma, A.; Jeon, Y.; Kwak, J. H.; Sessler, J. L.; Shabat, D.; Kim, J. S. Chemiluminescent Probe for the In Vitro and In Vivo Imaging of Cancers Over-Expressing NQO1. *Angew. Chem., Int. Ed.* **2019**, *58*, 1739−1743.
(49) An, R.; Wei, S.; Huang, Z.; Liu, F.; Ye, D. An Activatable Chemiluminescent Probe for Sensitive Detection of γ-Glutamyl Transpeptidase Activity in Vivo. *Anal. Chem.* **2019**, *91*, 13639−13646.
(50) Hananya, N.; Press, O.; Das, A.; Scomparin, A.; Satchi-Fainaro, R.; Sagi, I.; Shabat, D. Persistent Chemiluminescent Glow of Phenoxy-Dioxetane Luminophore Enables Unique CRET-Based Detection of Proteases. *Chem. - Eur. J.* **2019**, *25*, 14679−14687.
(51) Miranda-Apodaca, J.; Hananya, N.; Velázquez-Campoy, A.; Shabat, D.; Arellano, J. B. Emissive Enhancement of the Singlet Oxygen Chemiluminescence Probe after Binding to Bovine Serum Albumin. *Molecules* **2019**, *24*, 2422.
(52) Hananya, N.; Green, O.; Blau, R.; Satchi-Fainaro, R.; Shabat, D. A Highly Efficient Chemiluminescence Probe for the Detection of Singlet Oxygen in Living Cells. *Angew. Chem., Int. Ed.* **2017**, *56*, 11793−11796.
(53) Ryan, L. S.; Lippert, A. R. Ultrasensitive Chemiluminescent Detection of Cathepsin B: Insights into the New Frontier of Chemiluminescent Imaging. *Angew. Chem., Int. Ed.* **2018**, *57*, 622−624.

https://dx.doi.org/10.1021/acssensors.0c01393
ACS Sens. 2020, 5, 2925−2932

(54) Knox, H. J.; Hedhli, J.; Kim, T. W.; Khalili, K.; Dobrucki, L. W.; Chan, J. A Bioreducible N-Oxide-Based Probe for Photoacoustic Imaging of Hypoxia. *Nat. Commun.* **2017**, *8*, 1794.
(55) Knox, H. J.; Kim, T. W.; Zhu, Z.; Chan, J. Photophysical Tuning of N-Oxide-Based Probes Enables Ratiometric Photoacoustic Imaging of Tumor Hypoxia. *ACS Chem. Biol.* **2018**, *13*, 1838−1843.
(56) Zhou, E. Y.; Knox, H. J.; Liu, C.; Zhao, W.; Chan, J. A Conformationally Restricted Aza-BODIPY Platform for Stimulus-Responsive Probes with Enhanced Photoacoustic Properties. *J. Am. Chem. Soc.* **2019**, *141*, 17601−17609.
(57) McDonnell, S. O.; O'Shea, D. F. Near-Infrared Sensing Properties of Dimethlyamino-Substituted BF2−Azadipyrromethenes. *Org. Lett.* **2006**, *8*, 3493−3496.
(58) Grimm, J. B.; Sung, A. J.; Legant, W. R.; Hulamm, P.; Matlosz, S. M.; Betzig, E.; Lavis, L. D. Carbofluoresceins and Carborhodamines as Scaffolds for High-Contrast Fluorogenic Probes. *ACS Chem. Biol.* **2013**, *8*, 1303−1310.
(59) Grimm, J. B.; Gruber, T. D.; Ortiz, G.; Brown, T. A.; Lavis, L. D. Virginia Orange: A Versatile, Red-Shifted Fluorescein Scaffold for Single- And Dual-Input Fluorogenic Probes. *Bioconjugate Chem.* **2016**, *27*, 474−480.
(60) Grimm, J. B.; English, B. P.; Choi, H.; Muthusamy, A. K.; Mehl, B. P.; Dong, P.; Brown, T. A.; Lippincott-Schwartz, J.; Liu, Z.; Lionnet, T.; et al. Bright Photoactivatable Fluorophores for Single-Molecule Imaging. *Nat. Methods* **2016**, *13*, 985−988.
(61) Grimm, J. B.; Brown, T. A.; Tkachuk, A. N.; Lavis, L. D. General Synthetic Method for Si-Fluoresceins and Si-Rhodamines. *ACS Cent. Sci.* **2017**, *3*, 975−985.
(62) Zhou, X.; Lai, R.; Beck, J. R.; Li, H.; Stains, C. I. Nebraska Red: A Phosphinate-Based near-Infrared Fluorophore Scaffold for Chemical Biology Applications. *Chem. Commun.* **2016**, *52*, 12290−12293.
(63) Fang, Y.; Good, G. N.; Zhou, X.; Stains, C. I. Phosphinate-Containing Rhodol and Fluorescein Scaffolds for the Development of Bioprobes. *Chem. Commun.* **2019**, *55*, 5962−5965.
(64) Michie, M. S.; Götz, R.; Franke, C.; Bowler, M.; Kumari, N.; Magidson, V.; Levitus, M.; Loncarek, J.; Sauer, M.; Schnermann, M. J. Cyanine Conformational Restraint in the Far-Red Range. *J. Am. Chem. Soc.* **2017**, *139*, 12406−12409.
(65) Cosco, E. D.; Caram, J. R.; Bruns, O. T.; Franke, D.; Day, R. A.; Farr, E. P.; Bawendi, M. G.; Sletten, E. M. Flavylium Polymethine Fluorophores for Near- and Shortwave Infrared Imaging. *Angew. Chem., Int. Ed.* **2017**, *56*, 13126−13129.
(66) Pengshung, M.; Neal, P.; Atallah, T. L.; Kwon, J.; Caram, J. R.; Lopez, S. A.; Sletten, E. M. Silicon Incorporation in Polymethine Dyes. *Chem. Commun.* **2020**, *56*, 6110−6113.
(67) Green, O.; Eilon, T.; Hananya, N.; Gutkin, S.; Bauer, C. R.; Shabat, D. Opening a Gateway for Chemiluminescence Cell Imaging: Distinctive Methodology for Design of Bright Chemiluminescent Dioxetane Probes. *ACS Cent. Sci.* **2017**, *3*, 349−358.
(68) Green, O.; Gnaim, S.; Blau, R.; Eldar-Boock, A.; Satchi-Fainaro, R.; Shabat, D. Near-Infrared Dioxetane Luminophores with Direct Chemiluminescence Emission Mode. *J. Am. Chem. Soc.* **2017**, *139*, 13243−13248.
(69) Rainey, K. H.; Patterson, G. H. Photoswitching FRET to Monitor Protein−Protein Interactions. *Proc. Natl. Acad. Sci. U.S.A.* **2019**, *116*, 864−873.
(70) Chung, C. Y.-S.; Posimo, J. M.; Lee, S.; Tsang, T.; Davis, J. M.; Brady, D. C.; Chang, C. J. Activity-Based Ratiometric FRET Probe Reveals Oncogene-Driven Changes in Labile Copper Pools Induced by Altered Glutathione Metabolism. *Proc. Natl. Acad. Sci. U.S.A.* **2019**, *116*, 18285−18294.
(71) Albers, A. E.; Okreglak, V. S.; Chang, C. J. A FRET-Based Approach to Ratiometric Fluorescence Detection of Hydrogen Peroxide. *J. Am. Chem. Soc.* **2006**, *128*, 9640−9641.
(72) Zhang, X.; Xiao, Y.; Qian, X. A Ratiometric Fluorescent Probe Based on FRET for Imaging Hg2+ Ions in Living Cells. *Angew. Chem., Int. Ed.* **2008**, *47*, 8025−8029.
(73) Ai, H.-w.; Hazelwood, K. L.; Davidson, M. W.; Campbell, R. E. Fluorescent Protein FRET Pairs for Ratiometric Imaging of Dual Biosensors. *Nat. Methods* **2008**, *5*, 401−403.
(74) Hananya, N.; Eldar Boock, A.; Bauer, C. R.; Satchi-Fainaro, R.; Shabat, D. Remarkable Enhancement of Chemiluminescent Signal by Dioxetane-Fluorophore Conjugates: Turn-ON Chemiluminescence Probes with Color Modulation for Sensing and Imaging. *J. Am. Chem. Soc.* **2016**, *138*, 13438−13446.
(75) An, W.; Mason, R. P.; Lippert, A. R. Energy Transfer Chemiluminescence for Ratiometric PH Imaging. *Org. Biomol. Chem.* **2018**, *16*, 4176−4182.
(76) Lumpi, D.; Wagner, C.; Schöpf, M.; Horkel, E.; Ramer, G.; Lendl, B.; Fröhlich, J. Fibre Optic ATR-IR Spectroscopy at Cryogenic Temperatures: In-Line Reaction Monitoring on Organolithium Compounds. *Chem. Commun.* **2012**, *48*, 2451−2453.
(77) Kommreddy, A.; Bowsher, M. S.; Gunna, M. R.; Botha, K.; Vinod, T. K. Expedient Synthesis and Solvent Dependent Oxidation Behavior of a Water-Soluble IBX Derivative. *Tetrahedron Lett.* **2008**, *49*, 4378−4382.
(78) Chan, C.-H.; Wilbanks, C. C.; Makhatadze, G. I.; Wong, K.-B. Electrostatic Contribution of Surface Charge Residues to the Stability of a Thermophilic Protein: Benchmarking Experimental and Predicted pKa Values. *PLoS One* **2012**, *7*, No. e30296.

https://dx.doi.org/10.1021/acssensors.0c01393
ACS Sens. 2020, 5, 2925−2932